

# Are protons still dominant at the knee of the cosmic-ray energy spectrum?

M.Amenomori<sup>a</sup>, S.Ayabe<sup>b</sup>, D.Chen<sup>c</sup>, S.W.Cui<sup>d</sup>,  
 Danzengluobu<sup>e</sup>, L.K.Ding<sup>d</sup>, X.H.Ding<sup>e</sup>, C.F.Feng<sup>f</sup>, Z.Y.Feng<sup>g</sup>,  
 X.Y.Gao<sup>h</sup>, Q.X.Geng<sup>h</sup>, H.W.Guo<sup>e</sup>, H.H.He<sup>d</sup>, M.He<sup>f</sup>,  
 K.Hibino<sup>i</sup>, N.Hotta<sup>j</sup>, Haibing Hu<sup>e</sup>, H.B.Hu<sup>d</sup>, J.Huang<sup>k,\*</sup>,  
 Q.Huang<sup>g</sup>, H.Y.Jia<sup>g</sup>, F.Kajino<sup>l</sup>, K.Kasahara<sup>m</sup>, Y.Katayose<sup>c</sup>,  
 C.Kato<sup>n</sup>, K.Kawata<sup>k</sup>, Labaciren<sup>e</sup>, G.M.Le<sup>o</sup>, J.Y.Li<sup>f</sup>, H.Lu<sup>d</sup>,  
 S.L.Lu<sup>d</sup>, X.R.Meng<sup>e</sup>, K.Mizutani<sup>b</sup>, J.Mu<sup>h</sup>, K.Munakata<sup>n</sup>,  
 A.Nagai<sup>p</sup>, H.Nanjo<sup>a</sup>, M.Nishizawa<sup>q</sup>, M.Ohnishi<sup>k</sup>, I.Ohta<sup>j</sup>,  
 H.Onuma<sup>b</sup>, T.Ouchi<sup>i</sup>, S.Ozawa<sup>k</sup>, J.R.Ren<sup>d</sup>, T.Saito<sup>r</sup>,  
 M.Sakata<sup>l</sup>, T.Sasaki<sup>i</sup>, M.Shibata<sup>c</sup>, A.Shiomi<sup>k</sup>, T.Shirai<sup>i</sup>,  
 H.Sugimoto<sup>s</sup>, M.Takita<sup>k</sup>, Y.H.Tan<sup>d</sup>, N.Tateyama<sup>i</sup>, S.Torii<sup>t</sup>,  
 H.Tsuchiya<sup>u</sup>, S.Udo<sup>k</sup>, H.Wang<sup>d</sup>, X.Wang<sup>b</sup>, Y.G.Wang<sup>f</sup>,  
 H.R.Wu<sup>d</sup>, L.Xue<sup>f</sup>, Y.Yamamoto<sup>l</sup>, C.T.Yan<sup>k</sup>, X.C.Yang<sup>h</sup>,  
 S.Yasue<sup>n</sup>, Z.H.Ye<sup>o</sup>, G.C.Yu<sup>g</sup>, A.F.Yuan<sup>e</sup>, T.Yuda<sup>i</sup>,  
 H.M.Zhang<sup>d</sup>, J.L.Zhang<sup>d</sup>, N.J.Zhang<sup>f</sup>, X.Y.Zhang<sup>f</sup>, Y.Zhang<sup>d</sup>,  
 Yi.Zhang<sup>d</sup>, Zhaxisangzhu<sup>e</sup>, X.X.Zhou<sup>g</sup>,  
 (The Tibet AS $\gamma$  Collaboration)

<sup>a</sup>*Department of Physics, Hirosaki University, Hirosaki 036-8561, Japan*

<sup>b</sup>*Department of Physics, Saitama University, Saitama 338-8570, Japan*

<sup>c</sup>*Faculty of Engineering, Yokohama National University, Yokohama 240-8501, Japan*

<sup>d</sup>*Key Laboratory of Particle Astrophysics, Institute of High Energy Physics, Chinese Academy of Sciences, Beijing 100049, China*

<sup>e</sup>*Department of Mathematics and Physics, Tibet University, Lhasa 850000, China*

<sup>f</sup>*Department of Physics, Shandong University, Jinan 250100, China*

<sup>g</sup>*Institute of Modern Physics, South West Jiaotong University, Chengdu 610031, China*

<sup>h</sup>*Department of Physics, Yunnan University, Kunming 650091, China*

<sup>i</sup>*Faculty of Engineering, Kanagawa University, Yokohama 221-8686, Japan*

<sup>j</sup>*Faculty of Education, Utsunomiya University, Utsunomiya 321-8505, Japan*

<sup>k</sup>*Institute for Cosmic Ray Research, University of Tokyo, Kashiwa 277-8582,*

*Japan*

<sup>ℓ</sup>*Department of Physics, Konan University, Kobe 658-8501, Japan*

<sup>m</sup>*Faculty of Systems Engineering, Shibaura Institute of Technology, Saitama  
337-8570, Japan*

<sup>n</sup>*Department of Physics, Shinshu University, Matsumoto 390-8621, Japan*

<sup>o</sup>*Center of Space Science and Application Research, Chinese Academy of Sciences,  
Beijing 100080, China*

<sup>p</sup>*Advanced Media Network Center, Utsunomiya University, Utsunomiya 321-8585,  
Japan*

<sup>q</sup>*National Institute for Informatics, Tokyo 101-8430, Japan*

<sup>r</sup>*Tokyo Metropolitan College of Aeronautical Engineering, Tokyo 116-0003, Japan*

<sup>s</sup>*Shonan Institute of Technology, Fujisawa 251-8511, Japan*

<sup>t</sup>*Advanced Research Institute for Science and Engineering, Waseda University,  
Tokyo 169-8555, Japan*

<sup>u</sup>*RIKEN, Wako 351-0198, Japan*

---

## Abstract

A hybrid experiment consisting of emulsion chambers, burst detectors and the Tibet II air-shower array was carried out at Yangbajing (4,300 m a.s.l., 606 g/cm<sup>2</sup>) in Tibet to obtain the energy spectra of primary protons and heliums. From three-year operation, these energy spectra are deduced between 10<sup>15</sup> and 10<sup>16</sup> eV by triggering the air showers associated with a high energy core and using a neural network method in the primary mass separation. The proton spectrum can be expressed by a single power-law function with a differential index of  $-3.01 \pm 0.11$  and  $-3.05 \pm 0.12$  based on the QGSJET+HD and SIBYLL+HD models, respectively, which are steeper than that extrapolated from the direct observations of  $-2.74 \pm 0.01$  in the energy range below 10<sup>14</sup> eV. The absolute fluxes of protons and heliums are derived within 30% systematic errors depending on the hadronic interaction models used in Monte Carlo simulation. The result of our experiment suggests that the main component responsible for the change of the power index of the all-particle spectrum around  $3 \times 10^{15}$  eV, so-called “knee”, is composed of nuclei heavier than helium. This is the first measurement of the differential energy spectra of primary protons and heliums by selecting them event by event at the knee energy region.

*Key words:* cosmic rays,  $\gamma$ -family, neural network, proton, knee energy region

*PACS:* 98.70.Sa, 95.85.Ry, 96.40.De, 96.40.Pq

---

\* Corresponding author.

*Email address:* [huang@icrr.u-tokyo.ac.jp](mailto:huang@icrr.u-tokyo.ac.jp) (J.Huang).

## 1 Introduction

The energy spectrum of cosmic rays is described by a power-law function in a wide energy range from about  $10^{10}$  eV to  $10^{20}$  eV, however, it shows slight changes of the power-law index at several points. These break points of the power-law spectrum are assumed to be related to the origin, acceleration mechanism and propagation mechanism of cosmic rays in the Galaxy. One of the break points, in which the present paper is concerned, is traditionally referred to as the “knee” located around  $3 \times 10^{15}$  eV. Many experiments have reported [1] that the power-law indices below and above the knee approximately take the values  $-2.7$  and  $-3.1$ , respectively. Although existence of the knee has been well established experimentally, there are still controversial arguments on its origin. One of them is a possibility that acceleration mechanism could be less effective above the knee. Along with this line, there is a general consensus that stochastic shock acceleration at supernova blast waves could explain the cosmic-ray spectrum up to about  $Z \times 10^{14}$  eV [2], or perhaps even higher to  $Z \times 10^{15}$  eV [3], where  $Z$  denotes the atomic number, despite lack of direct evidence. Another argument attributes the knee structure to the leakage of the cosmic rays from the galaxy [4]. It is noted that both scenarios mentioned above give a rigidity-dependent cutoff for each chemical component leading to a heavy-enriched composition of primary cosmic rays at the knee. On the other hand, there is another approach in which cosmic rays around and beyond the knee are assumed to be of extra-galactic origin such as the active galactic nuclei [5] or gamma-ray bursts [6]. In this case, the primary chemical composition is expected to become proton-enriched. There have been some calculations of the primary cosmic-ray energy spectrum based on various models on the origin of the knee [7], but all of them are still under debate due to lack of detailed knowledge about the chemical composition around the knee.

Among primary cosmic rays, protons are the key component for understanding the origin of the knee. Direct measurements of primary cosmic rays on board balloons or satellites are the best ways, however, the energy region covered by them are limited up to  $10^{14}$  eV. The chemical composition of primary cosmic rays around the knee, therefore, has been studied with ground-based air-shower experiments and/or air Cherenkov telescopes. Since the sensitivity to the mass separation among cosmic-ray nuclei with ground-based experiments is limited, only gross features such as average mass number have been discussed. A lot of reports have so far been made on the energy spectrum as well as the chemical composition of primary cosmic rays, however, there are still serious disagreements among them especially on the chemical composition [8].

It is possible, however, to improve the sensitivity of an air shower experiment to the primary cosmic-ray mass separation by adding a function to observe

the energy-flow characteristics of air-shower cores at a high-mountain altitude. The Tibet hybrid experiment [9] was designed to detect  $\gamma$ -families in an air shower core by large-area emulsion chambers in coincidence with an accompanied air shower, where a bundle of energetic  $\gamma$ -rays and electrons detected by the emulsion chambers are called a  $\gamma$ -family, which is caused by a young air shower. Among primary cosmic rays, protons and heliums can penetrate deep into the atmosphere and produce a young air shower accompanied by a  $\gamma$ -family event most efficiently due to their longest interaction mean free paths in the air. Therefore, tagging an air shower with a  $\gamma$ -family event enriches the proton and helium component naturally. Another merit in doing a hybrid experiment in Tibet is that the atmospheric depth of the experimental site (4300 m a.s.l., 606 g/cm<sup>2</sup>) is close to the maximum development of the air showers with energies around the knee almost irrespective of the masses of primary cosmic rays. We can determine the primary cosmic-ray energy much less dependently upon the chemical composition [10] than those experiments at the sea level. Thus, the Tibet hybrid experiment enables us to measure the primary proton and helium differential energy spectra by selecting them event by event.

In this paper, we briefly report on the study of the energy spectra of the proton and helium components in cosmic rays around the knee energy region obtained with the Tibet hybrid experiment.

## 2 Experiment

The Tibet hybrid experiment, consisting of emulsion chambers (ECs), burst detectors (BDs) and the Tibet-II air-shower array (AS), composed of 221 scintillation counters each placed on a 15 m square grid with an enclosed area of 36,900 m<sup>2</sup> was operated at Yangbajing in Tibet during the period from November 1996 through August 1999 [9] and a total live time of 699.2 days.

The AS is used to measure the shower size and the arrival direction of each air shower. Any four-fold coincidence in the detectors is used as the trigger condition for air-shower events. The air shower direction can be estimated with an error smaller than 1°. The primary energy of each event is determined by the shower size ( $N_e$ ). The energy resolution is estimated to be 17% at energies around 10<sup>15</sup> eV by our simulation, almost independent of the interaction models used.

The ECs and the BDs are constructed near the center of the AS [11], and are used to detect high-energy air shower cores accompanied by air showers induced by primary cosmic rays with energies above  $\sim 10^{14}$  eV. The total area of ECs is 80 m<sup>2</sup>. The basic structure of each EC is a multilayered sandwich

of lead plates and X-ray films (FUJI X-RAY FILM TYPE 200) of  $40\text{ cm} \times 50\text{ cm}$  in area, where X-ray films are put every 1.0 cm of lead in the chamber. The X-ray films in ECs are replaced by new ones every year to reduce the background. The ECs are used to measure the energy, the position and the arrival direction of each  $\gamma$ -family shower with energies above 1 TeV. The BD with the same area are placed just below 4 ECs, namely, 4 ECs are set above one unit of the BD. Thus, 400 blocks of ECs and 100 BDs in total are used in this experiment. A burst event is triggered when any two-fold coincidence of signals from four photodiodes of each BD appears. When the BDs trigger an event, its accompanying air shower is simultaneously recorded. The BDs are used to measure the burst size  $N_b$  and the position of each air shower core. The arrival direction of the  $\gamma$ -family event is determined by the spatial reconstruction of the cascade showers in ECs, whose details are described in [12]. The matching between an AS and a BD event is made by their arrival time stamps, and the matching between a  $\gamma$ -family event in EC and the BD event is made by their positional correlation, and the matching between the  $\gamma$ -family event in EC and the AS event is made by their directional correlation.

In the following analysis, we present our results based on the ECs and AS data, as those obtained from the BDs data were published in the previous paper [11].

### 3 Simulation

We have carried out a detailed Monte Carlo (MC) simulation of air showers and  $\gamma$ -families using the simulation code CORSIKA (version 6.030) including QGSJET01 and SIBYLL2.1 hadronic interaction models [13]. From a point of view to check the dependence of the obtained results on the assumed primary cosmic-ray composition in MC, two primary composition models are examined as the input energy spectra, namely a heavy dominant (HD) and a proton dominant (PD) ones [9]. The energy spectrum of each component in the HD model has a rigidity-dependent break point of the power index with proton's knee around  $1.5 \times 10^{14}\text{ eV}$  leading to the dominance of the heavy component at the knee energy region. On the other hand, it is assumed in the PD model that light components are dominant up to the knee, in which every component has the same break point of the power index at the knee energy. In both models, the fraction and the power index of each component are determined by fitting to the fluxes of the elements obtained by direct observations below  $10^{14}\text{ eV}$ , and fitting the sum of the each element at higher energies to the all particle flux obtained by air shower experiments. Therefore, the difference between two models exists in the fraction of the elements above  $10^{14}\text{ eV}$ . The fractional contents of the assumed primary cosmic-ray flux models are listed in Table 1, together with those for making air showers accompanied by  $\gamma$ -

Table 1

Fractions of the proton(P), helium(He), medium(M) and iron(Fe) components in the assumed primary cosmic-ray spectrum of the HD and PD models(upper table), together with those for making air showers accompanied by  $\gamma$ -families (lower table) (see the Section 4).

Primary		HD				PD			
	Energy ( eV )	P	He	M	Fe	P	He	M	Fe
Generated	$10^{14} - 10^{15}$	22.6	19.2	36.0	22.2	39.0	20.4	31.2	9.4
(%)	$10^{15} - 10^{16}$	11.0	11.4	38.5	39.1	38.1	19.4	32.6	9.9

Model	Energy(eV)	P	He	M	Fe
QGSJET+HD	$10^{14}$ - $10^{15}$	$87.3\pm1.2$	$12.7\pm1.2$	0	0
(%)	$10^{15}$ - $10^{16}$	$58.9\pm0.9$	$27.2\pm0.8$	$12.3\pm0.9$	$1.6\pm0.3$
SIBYLL+HD	$10^{14}$ - $10^{15}$	$87.2\pm0.8$	$12.8\pm0.8$	0	0
(%)	$10^{15}$ - $10^{16}$	$57.3\pm0.7$	$24.2\pm0.7$	$16.9\pm0.8$	$1.6\pm0.3$
QGSJET+PD	$10^{14}$ - $10^{15}$	$91.8\pm0.8$	$8.2\pm0.8$	0	0
(%)	$10^{15}$ - $10^{16}$	$80.0\pm0.6$	$16.0\pm0.6$	$3.4\pm0.4$	$0.6\pm0.1$
SIBYLL+PD	$10^{14}$ - $10^{15}$	$94.2\pm0.6$	$5.8\pm0.6$	0	0
(%)	$10^{15}$ - $10^{16}$	$78.7\pm0.6$	$17.9\pm0.6$	$3.4\pm0.4$	$0.06\pm0.01$

families, where M denotes the sum of medium heavy elements between helium and iron. One can see from Table 1 that 100% of the  $\gamma$ -family events are induced by protons and heliums below  $10^{15}$  eV. At the higher energy range, however, the contribution of the other nuclei heavier than helium increases with the energy which amounts to around 15% and 4% in case of HD model and PD model, respectively. The method of the separation of primary mass groups using a neural network method is described in the next section.

The numbers of generated  $\gamma$ -family events satisfying the criteria described in the next section are 5252, 5926, 8588 and 7376 for the QGSJET+HD, QGSJET+PD, SIBYLL+HD and SIBYLL+PD models, respectively, which are more than 30 times greater than the experimental statistics.

## 4 Analysis

Shower spots registered by high-energy  $\gamma$ -rays or electrons in the X-ray films were automatically analyzed by using image scanners [12]. The  $\gamma$ -family events

are selected by imposing the conditions of  $E_{\gamma}^{th} = 4 \text{ TeV}$ ,  $N_{\gamma} \geq 4$ ,  $\sum_i E_{\gamma}^i \geq 20 \text{ TeV}$  and  $\langle R \rangle \geq 0.2 \text{ cm}$ , where  $E_{\gamma}^{th}$  is the minimum energy for a cascade shower,  $N_{\gamma}$  the number of cascade showers in a  $\gamma$ -family,  $\sum E_{\gamma}$  the sum energy of cascade showers in a  $\gamma$ -family and  $\langle R \rangle = (\langle R \rangle = \sum_i r_{\gamma}^i / N_{\gamma})$  the mean lateral spread in a  $\gamma$ -family. In this experiment, we observed a total of 177  $\gamma$ -family events, each of which is accompanied by an air shower with  $N_e > 2 \times 10^5$  corresponding approximately to  $5 \times 10^{14} \text{ eV}$  for a proton.

The separation of the primary mass is made with use of a feed-forward artificial neural network (ANN [14]) whose applicability to our experiment was well confirmed by the Monte Carlo simulation [15,11]. The first task of the ANN is to separate protons from everything else by training the network with a proton flag. As shown in Table 1, heliums are the main component of the contamination at lower energies while medium heavy component also contributes in higher energies depending on the primary composition. Then the second task of ANN is to separate a group of proton+helium from others above  $10^{15} \text{ eV}$  by training the network with a light element flag, i.e., a flag for proton or helium. Thus we can obtain helium spectrum by subtracting the number of proton events obtained in the first task from the proton+helium dataset.

We examine four cases, QGSJET + HD, QGSJET + PD, SIBYLL + HD and SIBYLL + PD models. The following six parameters are input to the ANN with 30 hidden nodes and 1 output unit, which are abbreviated to a 6 : 30 : 1 network <sup>1</sup> : (1)  $\sum E_{\gamma}$  in ECs, (2)  $N_{\gamma}$  in ECs, (3)  $\langle R \rangle$  in ECs, (4) the mean energy-flow spread  $\langle ER \rangle = \sum_i E_{\gamma}^i r_{\gamma}^i / N_{\gamma}$  in ECs, where  $E_{\gamma}^i$  and  $r_{\gamma}^i$  are the energy of each cascade shower in the  $\gamma$ -family and its distance from the energy-weighted family-center, respectively, (5) the air shower size  $N_e$  in AS, and (6)  $\sec \theta$ , where  $\theta$  is the zenith angle of the arrival direction.

One MC data set was generated for each of the four models and divided into two subsets; the one is used for training the ANN, and the other for estimating the ability of the ANN to classify the nuclear species. Then, the training MC data subset is fed to the ANN in a number of training cycles of 2000. <sup>2</sup> To train the ANN in separating protons from others, the input patterns for protons and other nuclei are set to 0 and 1, respectively. After the training, the another MC data subset is used to estimate the purity and the selection efficiency of protons. Then, the ANN output pattern value ( $T$ ) is a real number from 0 to 1. The  $T$  distributions in the QGSJET+HD model is presented in Fig. 1, together with the experimental data. One can see that the experimental data is in a good agreement with the MC prediction, and

<sup>1</sup> We compared the results from various number of hidden nodes and found the results are not changed when we use the number of hidden nodes greater than 20.

<sup>2</sup> The training curve becomes stable at number of training cycles 500.

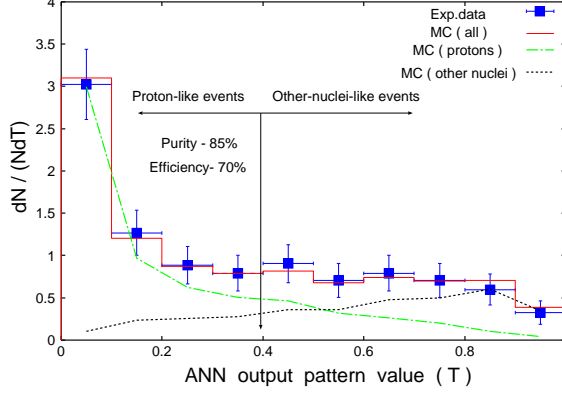


Fig. 1. ANN output pattern value ( $T$ ) distributions compared with MC (QGSJET+HD model). Used symbols are ; experimental data (the closed squares), MC:all (the solid-red histogram), MC:protons (the dash-dotted green line), MC:other nuclei (the dotted-black line).

that the proton-induced events are clearly separated from other nuclei.<sup>3</sup> We define a critical value of  $T$  to separate protons from others requiring the high purity, which reduces the effect of the contamination, and the high selection efficiency of the proton events, which reduces the statistical error. Since these two factors are of the competing nature, the purity and the selection efficiency are calculated as a function of the critical value  $T_c$  and its value is set as 0.4 where average purity and selection efficiency over whole energy range are greater than approximately 85% and 70% for all models, respectively. It was confirmed that the final result does not depend on the different choice of the  $T_c$  around 0.4. The high value of the purity as listed in Table 2 and their mutual deviation among different models in the same energy interval being within 4% assures us the quality of the proton selection.

Finally, we obtained 111, 111, 112, 112 proton-like events out of 177 observed events after the  $\gamma$ -family selection based on the QGSJET+HD, QGSJET+PD, SIBYLL+HD and SIBYLL+PD models, respectively, among which 110 events are identical and one event belongs only to QGSJET analysis and two events belong only to SIBYLL analysis.

<sup>3</sup> We also examined the QGSJET+PD, SIBYLL+HD and SIBYLL+PD models, obtaining similar results to the ones as shown in Fig. 1, for the selected events are already mostly proton and helium origin in all models as shown in Table 1. Of course there are some differences between HD model and PD model, reflecting the degree of the contamination, however, it is not large enough to rule out one of them because of experimental statistical errors. This figure demonstrates how the proton-induced events are separated from those induced by other nuclei.



Table 2

The purity of the selected events by  $T < 0.4$ .

Model	Energy(eV)	Purity(%)	
		HD	PD
QGSJET	$10^{14}$ - $10^{15}$	$96.7 \pm 0.7$	$97.4 \pm 0.4$
	$10^{15}$ - $10^{16}$	$83.1 \pm 1.6$	$86.7 \pm 0.8$
SIBYLL	$10^{14}$ - $10^{15}$	$96.2 \pm 0.5$	$97.3 \pm 0.3$
	$10^{15}$ - $10^{16}$	$82.8 \pm 1.2$	$86.1 \pm 0.7$

## 5 Results and Discussions

In Fig. 2, we show the measured primary cosmic-ray proton energy spectra assuming the two interaction models (QGSJET and SIBYLL) and two primary composition models (HD and PD), together with the results from other experiments. As seen in Fig. 2, the present results assuming the HD and PD models in the simulation are in a good agreement with each other within the statistical errors. The measured proton energy spectra can be expressed by a single power-law function of a differential form  $J(E)(\text{m}^{-2} \cdot \text{s}^{-1} \cdot \text{sr}^{-1} \cdot \text{GeV}^{-1}) = A \times 10^{-13} \times (\frac{E}{10^6 \text{GeV}})^{-B}$ , where  $(A, B)$  is  $(4.56 \pm 0.46, 3.01 \pm 0.11)$ ,  $(4.14 \pm 0.44, 3.08 \pm 0.11)$ ,  $(3.21 \pm 0.34, 3.05 \pm 0.12)$  and  $(3.24 \pm 0.34, 3.08 \pm 0.12)$  based on the QGSJET+HD, QGSJET+PD, SIBYLL+HD and SIBYLL+PD models, respectively, where the errors quoted are the statistical ones. The error in the spectral index is statistics dominant, while that in the absolute flux value is model-dependence dominant. For the absolute flux value, the QGSJET model gives approximately 30% higher flux than the SIBYLL model. This can be mainly attributed to the difference of Feynman  $x_F$ -distribution of charged mesons between QGSJET and SIBYLL model in the very forward region at a collision [13]. The Feynman  $x_F$ -distribution in the SIBYLL model is harder than that in the QGSJET model in the  $x_F > 0.2$  region, so that the generation efficiency of  $\gamma$ -families by the former model becomes higher than the latter, resulting in a lower proton flux in the case of the SIBYLL model. As compared in Fig. 2, the present results are consistent with those obtained by the burst detectors in this experiment within 25% [11]. This implies that the systematic energy-scale uncertainty in our experiment is estimated to be 10% level. A solid straight line with the power index  $-2.74$  drawn in Fig. 2 is the best fitted line for the data points in the energy region below  $10^{14}$  eV observed by recent direct measurements [22], which is harder than the indices of our proton spectra.

Thanks to its light mass, the helium component can also trigger our hybrid experiment although the efficiency at  $10^{15}$  eV is about 4 times lower than the case of protons. The ANN method is again applied to obtain the helium spec-

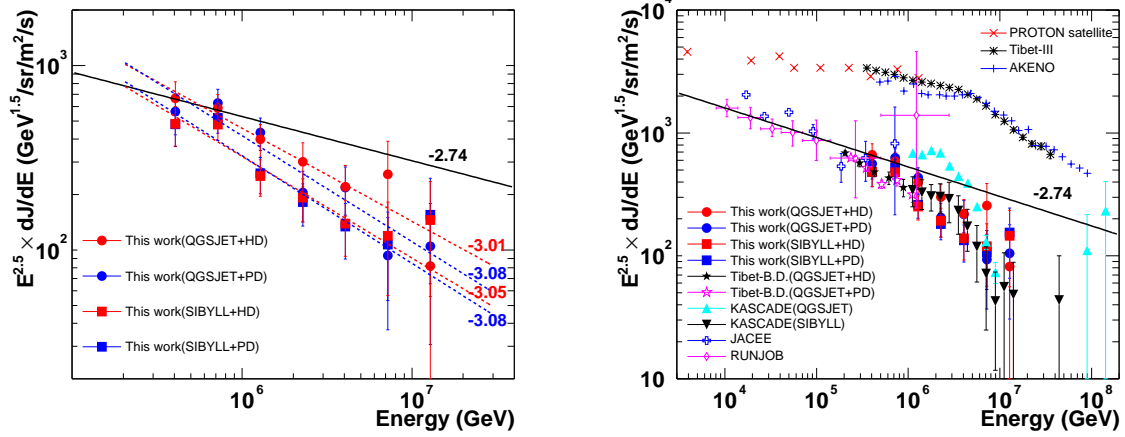


Fig. 2. Energy spectra of primary cosmic-ray protons obtained by the present experiment (a) and they are compared with other experiments (b): Tibet-B.D.[9], KASCADE[16], JACEE[17] and RUNJOB[18]. The all-particle spectra are from the experiments : PROTON satellite[19], Tibet-III[20] and AKENO[21]. For the solid line with the power index  $-2.74$ , see the text.

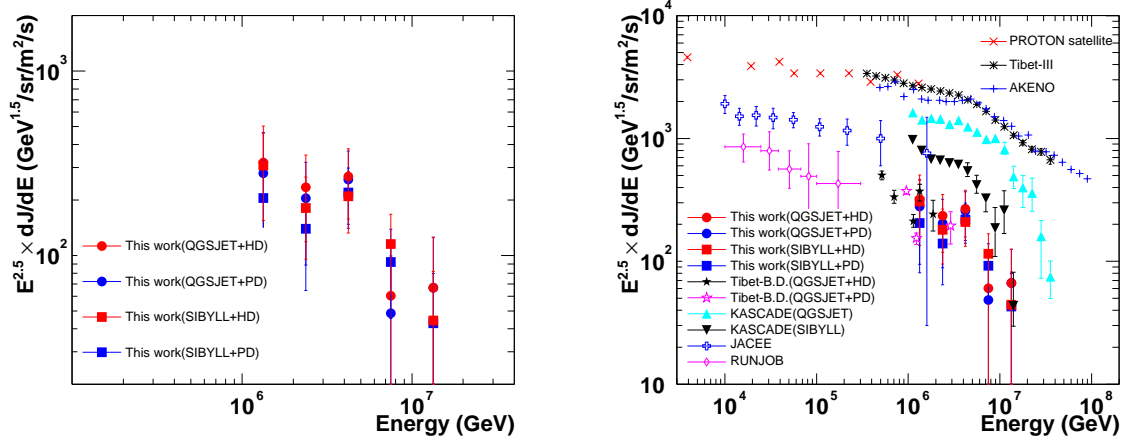


Fig. 3. Energy spectra of primary cosmic-ray helium nuclei obtained by the present experiment (a) and they are compared with other experiments (b)

trum over the energy  $10^{15}$  eV. Because of the training algorithm of ANN, it is not possible to train the network to separate heliums from others directly, for the helium mass is between protons and other heavy nuclei and the characteristics of the helium event is smeared out by the fluctuation tail from the both sides. Therefore we train the network to separate light component (proton or helium) from other nuclei, by assigning 0 to light component and 1 to other nuclei. The critical value  $T_c$  to select light component is set as 0.2 where the selection efficiency reaches to 70% and the purity is 93% for all models. Then, the helium spectra can be obtained by subtracting the number of protons, which are previously obtained by proton-training, from the number of proton+helium events. Above mentioned procedure was applied on each energy

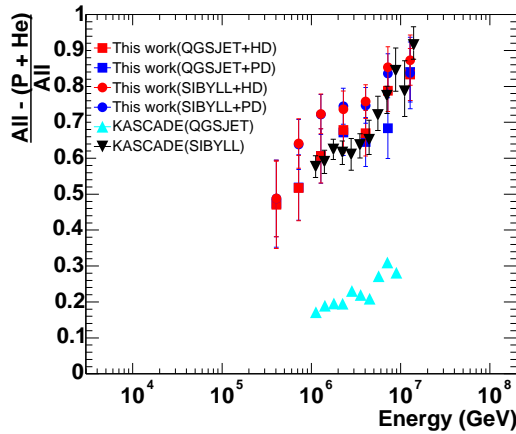


Fig. 4. Fraction of the primary cosmic-rays heavier than helium nuclei obtained by assuming the QGSJET and SIBYLL interaction models. Our results are compared with those by the KASCADE experiment[16].

bin to obtain the energy spectra of heliums and the result is shown in Fig. 3, where the same dependence of the absolute intensity on the interaction models is seen as in the case of proton spectra.

We can also estimate the fraction of the nuclei heavier than helium in cosmic rays around the knee using the proton+helium spectra and the all-particle energy spectrum obtained by the Tibet air shower array [20]. Shown in Fig. 4 is the fraction of primary cosmic rays heavier than helium nuclei assuming the QGSJET model and the SIBYLL model which are compared with those obtained recently by the KASCADE experiment [16]. Our results using 4 kinds of simulation models commonly indicate the average mass of primary cosmic rays is going up around the knee, towards the direction of heavy dominance. On the other hand, the KASCADE results which measures both air shower size ( $N_e$ ) and muon size ( $N_\mu$ ) to deduce the energy spectrum of separate mass groups from the all-particle energy spectrum, strongly depend on the interaction models. The muon size contained in the air shower depends on the number of charged pions produced in the central and backward region (in the center of mass system) in the collisions of primary cosmic rays on air nuclei, which has a sizeable uncertainties experimentally as well as theoretically and is largely dependent on the interaction models. From this point of view, the size of low-energy muons  $N_\mu$  may not be a suitable parameter for separating the air showers into different primary mass groups.

## 6 Summary

A hybrid experiment of emulsion chamber and air-shower array was successfully done at Yangbajing in Tibet to study the primary cosmic rays around the knee energy region. Using the events observed simultaneously in the emulsion chamber and the air-shower array, and applying a neural network analysis to this data set, we obtained the energy spectrum of primary protons in the energy range from  $4 \times 10^{14}$  eV to  $10^{16}$  eV. The spectrum observed can be represented by the power-law fit and the power indexes are estimated to be  $-3.01 \pm 0.11$  and  $-3.05 \pm 0.12$  for the spectra obtained using the ANN trained by the QGSJET+HD and SIBYLL+HD events, respectively, which are steeper than that extrapolated from the direct observations of  $-2.74 \pm 0.01$  in the energy range below  $10^{14}$  eV. The absolute fluxes of protons was derived within 30% systematic errors depending on the hadronic interaction models adopted in the Monte Carlo simulation. We also estimated the primary helium spectrum at energies above  $10^{15}$  eV, which has almost same spectral slope with the proton spectrum.

We further obtained the result that the fraction of the nuclei heavier than helium in the primary cosmic rays around the knee region, which was estimated using the proton+helium spectrum and the all-particle spectrum observed with the Tibet experiment, increases with increasing primary energy. This strongly suggests that the main component responsible for making the knee structure in the all-particle energy spectrum is the nuclei heavier than the helium component.

This is the first measurement of the differential energy spectra of primary protons and heliums by selecting them event by event. In the very near future, we will start a new high-statistics hybrid experiment in Tibet to clarify the main component of cosmic rays at the knee. The new experiment is able to observe the air shower cores induced by heavy components around and beyond the knee, where direct measurements are inaccessible because of their extremely low fluxes [23].

## Acknowledgments

This work is supported in part by Grants-in-Aid for Scientific Research on Priority Area (712) (MEXT) and also for Scientific Research (JSPS) in Japan, and by the Committee of the Natural Science Foundation and by the Chinese Academy of Sciences in China. The support of the JSPS (J.H., grant No. P03025) is also acknowledged.

## References

- [1] Cosmic-ray energy spectrum obtained by many air shower experiments is compiled by J.R. Hörandel[8].
- [2] P.O. Lagage, C.J. Cesarsky, et al., *Astron. Astrophys.* **118** (1983) 223.
- [3] J.R. Jokipii, *ApJ* **313** (1987) 842.
- [4] B. Peters, *Nuovo Cimento* **22** (1961) 800.
- [5] R.J. Protheroe, A.P. Szabo, et al., *Phys. Rev. Lett.*, **69** (1992) 2885.
- [6] R. Plaga, *New Astron.*, **7** (2002) 317.
- [7] J.R. Hörandel, *Astropart. Phys.*, **21** (2004) 241.
- [8] J.R. Hörandel, *Astropart. Phys.*, **19** (2003) 193.
- [9] M. Amenomori, S. Ayabe, Caidong, et al., *Phys. Rev. D* **62** (2000) 112002.
- [10] M. Amenomori, Z. Cao, B.Z. Dai, et al., *ApJ*. **461** (1996) 408.
- [11] M. Amenomori, S. Ayabe, Caidong, et al., *Phys. Rev. D* **62** (2000) 072007.
- [12] S. Ozawa, et al., *Nucl. Instrum. Methods, Phys. Res.* **A523** (2004) 193.
- [13] D. Heck, et al., Report **FZKA 6019**, 1998 ; [http://www-ik3.fzk.de/~heck/corsika/physics\\_description/corsika\\_phys.html](http://www-ik3.fzk.de/~heck/corsika/physics_description/corsika_phys.html).
- [14] L. Lonnblad, et al., *Comp. Phys. Com.*, **81** (1994) 185.
- [15] C.S. Zhang, T. Yuda, K. Kasahara, *Nucl. Instr. Methods, Phys. Res.* **A376** (1996) 263.
- [16] K.-H. Kampert, T. Antoni, W.D. Apel, et al., *Acta Phys. Polon. B*, **35** (2004) 1799; A. Haungs, T. Antoni, W.D. Apel, et al., *astroph/0312295*.
- [17] K. Asakimori, T.H. Burnett, M.L. Cherry, et al., *ApJ* **502** (1998) 278.
- [18] A.V. Apanasenko, V.A. Sukhadolskaya, V.A. Derbina, et al., *Astropart. Phys.* **16** (2001) 13.
- [19] N.L. Grigorov, Yu.V. Gubin, B.M. Jakovlev, et al., *Proc. 12th Int. Cosmic Ray Conf. (Hobart)*, **5** (1971) 1746.
- [20] M. Amenomori, S. Ayabe, S.W. Cui, et al., *Proc. 28th Int. Cosmic Ray Conf. (Tsukuba)*, **1** (2003) 143.
- [21] M. Nagano, T. Hara, Y. Hatano, et al., *J. Phys. G* **10** (1984) 1295.
- [22] T.K. Gaisser, et al., *Proc. 27th Int. Cosmic Ray Conf. (Hamburg)*, **5** (2001) 1643.
- [23] X.W. Xu, T. Yuda, L.K. Ding, et al., *J. Phys. G : Nucl. Part. Phys.*, **29** (2003) 719.